Developing high strength Al-Si-Mg filler metals for aluminum fusion welding

Mohamed Ahmed[1], Mousa Javidani[1], Fatemeh Mirakhorli[2], Alexandre Maltais[3], X.-Grant Chen[1]

[1] Department of Applied Science, University of Québec at Chicoutimi, Saguenay, Québec, G7H 2B1, Canada

[2] National Research Council of Canada, Saguenay, Québec, G7H 8C3, Canada

[3] Arvida Research and Development Center, Rio Tinto Aluminum, Saguenay, Québec, G7S 4K8, Canada

Abstract

The 4xxx series of aluminum fillers are extensively used in aluminum welding owing to their excellent weldability, high cracking resistance, and low melting point. However, joints welded with commercial AA4043 fillers experience low mechanical strength. Therefore, we investigated the performance and mechanical strength of joints welded using newly developed Al-Si-Mg filler metals with different Mg contents (0.6–1.4 wt.%). AA6061-T6 plates were welded as the base metal using a gas metal arc welding process. The microstructures of the welded samples were characterized using optical microscopy, scanning electron microscopy, and transmission electron microscopy. The mechanical properties were characterized by microhardness and tensile testing. The results revealed that the new filler metals exhibited weldability similar to that of the ER4043 reference filler. The Mg concentration in the fusion zone of the new fillers was much higher than that of the reference filler. In the as-welded condition, all the fractures occurred outside the fusion zone. Therefore, all the welded samples exhibited similar mechanical strength, much lower than the base metal. After applying the post-weld heat treatment, the mechanical strength of all joints, regardless of the Mg content, reached the same level as the base metal and achieved 100% welding efficiency. Furthermore, the fusion zones were much stronger than the base metal and fusion zone of the reference filler using the new fillers with high Mg content, thus indicating their significant potential for welding high-strength aluminum structures.

Keyword: Aluminum fusion welding; Al-Si-Mg filler metals; Magnesium content; Fusion zones; Mechanical strength of joints.

1. Introduction

The demand for high-strength, weldable 6xxx series Al products is continuously increasing in various transportation industries (Ref 1). The mechanical properties of 6xxx series Al alloys are primarily driven by the number density and volume fraction of metastable Mg_2Si precipitates. Therefore, the chemical composition (particularly the Mg and Si content) and applied heat treatment process are critical parameters for achieving the desired mechanical properties (Ref 2,3). Furthermore, since 6xxx series Al products are widely used in car bodies, they are mostly required to be joined by welding. Various welding techniques have been developed to join aluminum components, such as gas metal arc welding (GMAW), laser beam welding (LBW), and friction stir welding (FSW) (Ref 4,5). Heat-treatable Al-based alloys (i.e., 6xxx alloys) encounter several weldability problems during fusion welding. These include lower strength of the fusion zone (FZ), cracking during welding, reduction of the mechanical strength in the heat-affected zone (HAZ), and high porosity of the weld metal. These defects are related to the filler metal chemistry, propensity towards cracking, and the welding process parameters (Ref 6,7).

Commercial Al-Si-based AA4043 weld wires have been widely used for the general-purpose welding of 6xxx Al products. This filler metal is characterized by high fluidity and high resistance towards weld/solidification cracking. However, as there is no strengthening element (mainly Mg to precipitate Mg_2Si) in the AA4043 filler metal, the mechanical properties of the joints are strongly dependent on dilution with the base metal (Ref 7). During the fusion welding process, the Mg content of the 6xxx base metal diffuses to the weld bead, thus contributing to strengthening via Mg_2Si precipitation hardening. However, in many situations, the dilution ratio between the base metal and filler wire can fluctuate, influencing the strength of the joints (Ref 6).

To improve the properties of weldments, Babu *et al*. (Ref 8) added 0.2 and 0.75 wt.% Sc to the AA4043 filler, observing an apparent grain refinement in the weldment when the Sc content was above the hypereutectic composition. In another study by Babu *et al*. (Ref 9), TiB_2 was added to the AA4043 fillers as a grain refiner, and

the microhardness (HV) of the weldments improved by approximately 20%. The Mg-containing and heat-treatable AA4643 filler metal was also designed to resolve the strengthening variation related to the dilution phenomenon. However, the AA4643 filler still requires dilution from the base metal (approximately 20%) to obtain optimum mechanical properties. In addition, as the AA4643 filler has a lower Si content relative to the AA4043 filler, it has lower fluidity, lower fatigue life, and is more susceptible to hot cracking (Ref 6). Later, AA4943 filler metal, with increased Mg content up to 0.5 wt.%, was developed to provide consistently higher tensile, yield, and shear strength relative to the AA4043 and AA4643 fillers while maintaining the same welding and corrosion characteristics as the AA4043 filler (Ref 6). Although AA4943 filler metal exhibits acceptable strength relative to its conventional 4xxx series counterparts, the increasing demand to develop high-strength weldable Al products necessitates the development of new filler metals. In addition, the influence of Mg, a major alloying element in filler metals, on the mechanical properties of the joints in 6xxx alloys has never been systematically investigated.

Further improvement in the mechanical strength of the joints would also enable manufacturers to decrease the size of fillet welds without compromising strength (Ref 7). Reducing the fillet size could potentially improve welding productivity by reducing the volume of weld wires used and welding process time. In addition, the reduced weld size/thickness could reduce weldment distortion. The objective of the present study is to develop a new generation of 4xxx series filler metals for aluminum fusion welding to obtain high-strength joints with consistent properties. High Mg additions (0.6–1.4 wt.%) were added to the filler metals, and their impact on the weldability, microstructure, and mechanical properties of AA6061 weldments was investigated.

2. Experimental procedure

The experimental flow chart is illustrated in Fig. 1. Direct chill (DC) cast billets (diameter of 101 mm) with varying Mg content were prepared to develop new weld wires. After homogenization at 530 °C for 10 h, the DC cast billets were transformed into weld wires (diameter of 1.5 mm) via extrusion and wiredrawing processes. The three experimental filler metals containing 0.6, 1, and 1.4% Mg were denoted as Mg0.6, Mg1, and Mg1.4, respectively. A commercial ER4043 weld wire was used as the reference filler metal. The AA6061-T6 plates, as the base metal (BM), were cut into 300 mm × 100 m × 2 mm sections and prepared in a butt joint configuration with a gap of 0+0.1 mm (Ref 10). GMAW was used to join the plates using a Fronius Transpulse Synergic 5000-CMT welding machine mounted on a Motoman UP50N robot. The chemical compositions of the filler wires and the base metal are listed in Table 1. The welding process was conducted with the following parameters: voltage of 21.6 ±0.3 V, current of 98 ±1 A, positive direct current electrode, 0.8 m/min as the travel speed, 3m/min as the wire feeding rate, and 100% Ar shielding gas with a flow rate of 24 L/min.

The welded plates were first examined by X-ray radiography tests (XRT) to verify macro-processing defects such as large porosities and cracks in weldments. After the XRT analysis, the welded plates were divided to the high porosity zone and the low porosity zones. At least four samples from the low porosity zones for each filler joints were polished and examined using the optical microscopy. A total of 20 images were taken from each sample at 50x and analyzed using the ImageJ software. The area fraction of porosity was calculated and the average value of the porosity was taken. Welded samples were prepared using a standard metallographic procedure to examine the microstructural evolution. The microstructures were observed using optical microscopy (OM), scanning electron microscopy (SEM, Jeol JSM-6480LV), and transmission electron microscopy (TEM, Jeol JEM-2100). The welded plates were subjected to post-weld heat treatment (PWHT): 1) solution treatment at 530 °C for 1 h followed by water quenching at ambient temperature, and 2) artificial aging at 170 °C for 6 h. The mechanical properties of the weldments in the as-welded (AW) and PWHT conditions were evaluated using HV and tensile tests. The Vickers microhardness of the joints was measured on polished samples using an NG-1000 CCD microhardness tester with a load of 50 g and a dwell time of 20 s. The tensile properties of the welded samples were measured using an Instron 8801 servo-hydraulic unit with a crosshead speed of 1 mm/min. An extensometer with a 25 mm gauge length was used to measure the strain. Two types of tensile samples were prepared: standard and double-edge notched samples, as shown in Fig. 2. At least five samples were obtained for each condition, and the average value was reported.

The polished samples were etched in a solution of 0.5% HF for 5 s to reveal the boundaries between the FZ and HAZ. Identifying the FZ enabled the calculation of the dilution ratio of fillers with BM at the FZ using the equation (Ref 11): dilution ratio = A/(A+B+C)%, where A, B, and C correspond to the cross-sectional areas of the melted BM, weld cap, and weld root reinforcement, respectively (see Fig. 3). The calculated dilution ratio was

approximately 56% for all welded joints; based on this ratio, the chemical compositions of the FZs were calculated (Table 2).

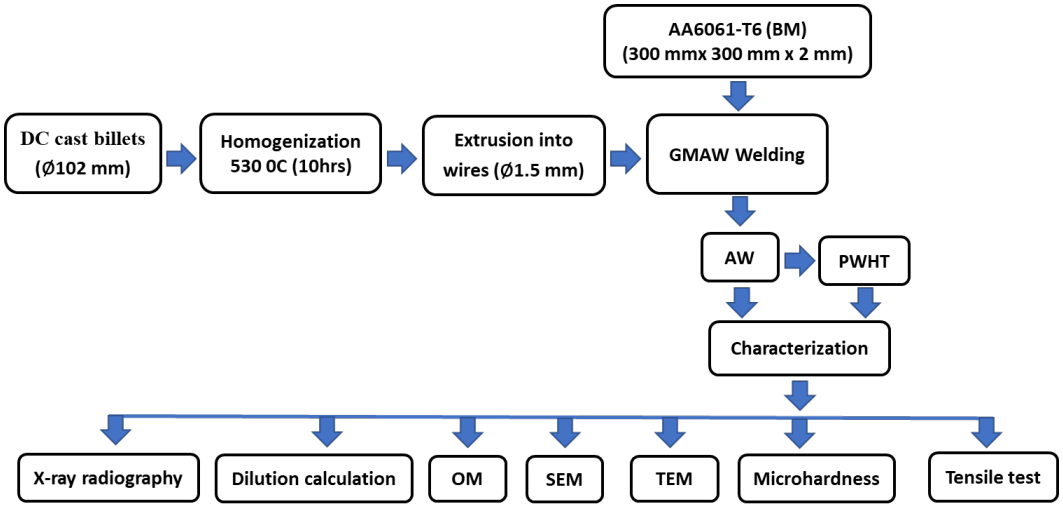

Figure 1: Flow chart of the experimental procedure.

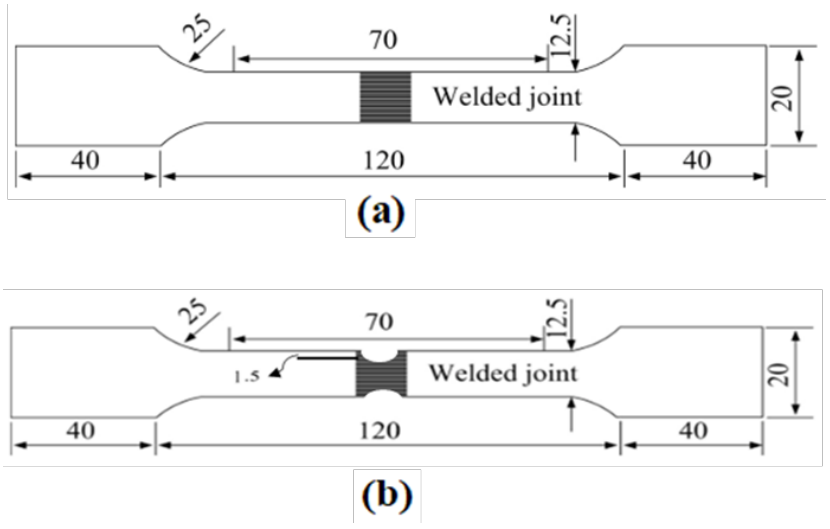

Figure 2: Dimension of the tensile samples for (a) standard and (b) double-edge notched samples.

Table 1: Chemical compositions of the base metal and filler metals (wt.%)

ID	Si	Fe	Mn	Mg	Cu
BM (base)	0.52	0.18	0.11	1.05	0.25
ER4043	5.5-6	<0.8	<0.05	<0.05	<0.3
Mg0.6	6.2	0.14	0.5	0.61	0.001
Mg1	6.2	0.15	0.52	1.04	0.001
Mg1.4	6.25	0.15	0.48	1.43	0.001

Table 2: The chemical compositions of the FZs calculated after dilution (wt.%)

Filler	Si	Fe	Mn	Mg	Cu
ER4043	2.478	0.171	0.070	0.599	0.140
Mg0.6	3.009	0.159	0.279	0.835	0.135
Mg1	3.009	0.163	0.288	1.025	0.135
Mg1.4	3.031	0.163	0.271	1.196	0.135

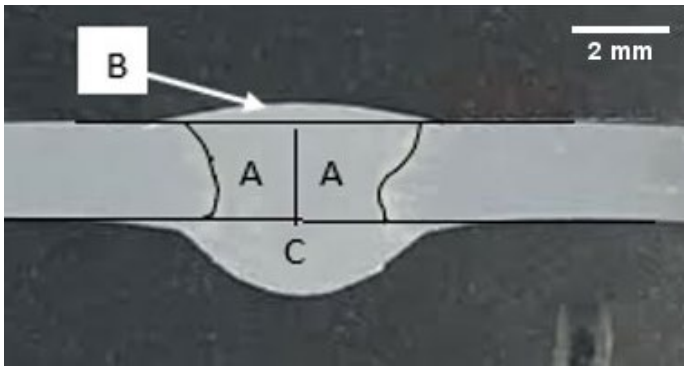

Figure 3: Macro view of a typical joint cross section for the dilution calculation.

3. Results and discussion

3.1 Weld geometry and imperfection

All weld plates were initially scanned by XRT to verify the integrity of the weld bead and the presence of macro imperfections, such as porosity and cracks. The XRT results showed no signs of slag inclusions, oxides, cracks, lack of fusion, or incomplete penetration for all welded plates, indicating similar weldability of the new filler metals and the reference ER4043 filler. Two zones, with high and low porosity levels, were observed along the weld bead, as shown in Fig. 4. As filler wires were not the commercial grades (manufactured at our laboratories), their surface was not perfectly smooth. Although in the preliminary tests it was tried to optimize the welding process parameters, the final welds in some regions could be influenced by the filler wire quality, and hence generated weld defects (like porosity) in certain zones, which named as high porosity zones. The weld cross-sections were extracted from the steady-state region of the weld in the low porosity zones. Based on the macroscopic images, no undercuts on the top or root surfaces were detected. Excessive penetration at the root side was less than 2 mm, passing the stringent quality level B (≤3 mm) based on the ISO 10042:2005(E) standard (Ref 12). The porosity content of the low porosity zones, verified by XRT and metallographic analysis, was less than 1%, passing the stringent quality level B (≤1%) based on the ISO 10042:2005(E) standard. Consequently, all samples used for microstructure characterization and mechanical property evaluation were prepared from low-porosity zones.

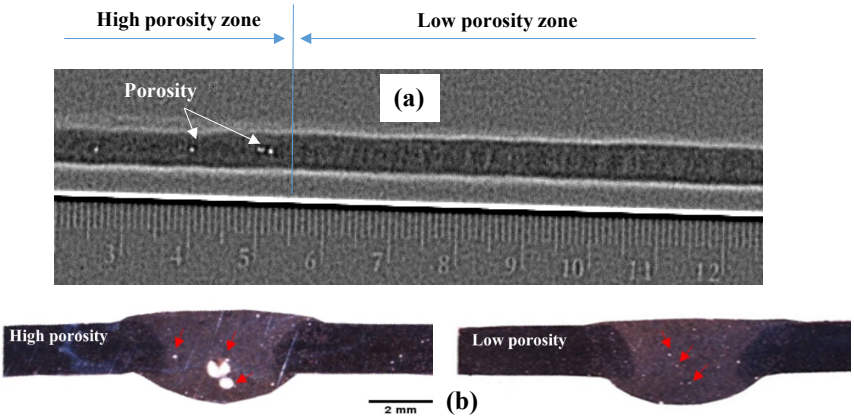

Figure 4: (a) XRT image of the weld and (b) macroscopic views of the low and high porosity zones (pores are indicated with red arrows).

3.2 Microstructures

3.2.1 As-welded microstructure

The grain morphologies in the BM, HAZ, and FZ were analyzed using OM, and the results are presented in Fig. 5. The BM (i.e., the as-received 6061-T6 plates) comprise coarse grains (average grain size of 70 µm) partially elongated in the rolling direction (Fig. 5(a)). Fine and equiaxed grains with an average size of 40 µm were observed in the HAZ (Fig. 5(b)); grains in the HAZ were subjected to static recrystallization owing to the heat input during the GMAW process. The fusion boundary between the HAZ and FZ revealed epitaxial growth of the columnar grains. The FZ was composed of dendritic equiaxed grains (average grain size of 130 µm), as shown in Fig. 5(c). The second dendrite arm space (SDAS) of the FZ was also similar (~16 µm) in all joints. These results indicate that constant weld parameters and similar solidification rates were applied to all welds, which were not influenced by the variation in the Mg content of the fillers.

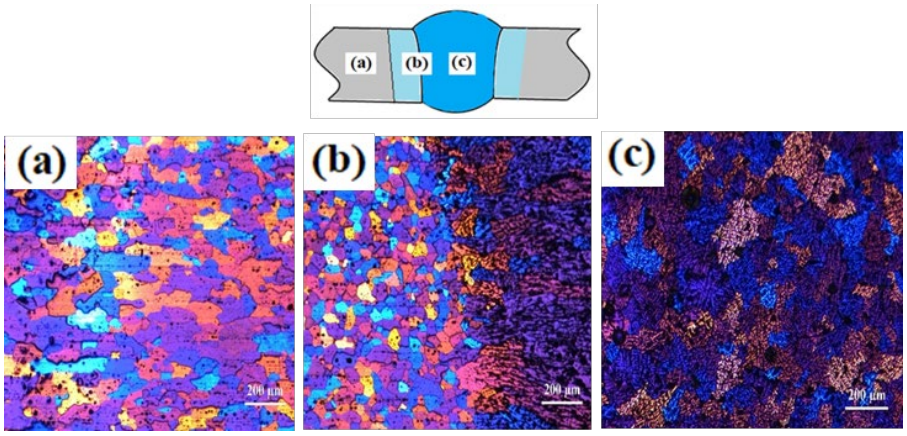

Figure 5: Grain morphology of the (a) BM, (b) HAZ, and (c) FZ in the joints welded with Mg1.4 filler.

The microstructure of the FZ was first calculated using the ThermoCalc software under Scheil conditions, using diluted FZ chemical compositions (Table 2). The predicted microconstituents and the corresponding mass fractions of the different phases in the ER4043 and Mg1.4 samples are shown in Fig. 6. The microconstituents in the FZ of both samples were α-Al, Si, Mg_2Si, α-Al(FeMn)Si, and β-AlFeSi. As shown in Fig. 6, the main differences between these two samples were the content and formation temperatures of Mg_2Si and the Fe-bearing intermetallics (i.e., β-AlFeSi and α-Al(FeMn)Si). Owing to the higher Mg content in the FZ of the Mg1.4 joints, the mass fraction of the Mg_2Si phase was considerably higher than the ER4043 joints (1.1 *vs*. 0.4%). Furthermore, considering the higher Mn content in the new fillers, the Fe-bearing intermetallics formed were mostly α-Al(FeMn)Si in the Mg1.4 joints rather than β-AlFeSi, as in the ER4043 joints.

The microstructures of the FZ of the ER4043 and Mg1.4 joints were further analyzed by SEM (Fig. 7). The principal microconstituents observed in both samples were α-Al, Si, Mg_2Si, α-Al (FeMn) Si, and β-AlFeSi, consistent with the predicted results (Fig. 6). Although the Mg content of the ER4043 filler was negligible (>0.05 %), the FZ of the joints contained a small amount of Mg_2Si particles (~0.2%) due to dilution with the BM. The area fraction of Mg_2Si particles increased to 0.28, 0.5, and 0.6% in the Mg0.6, Mg1, and Mg1.4 joints, respectively.

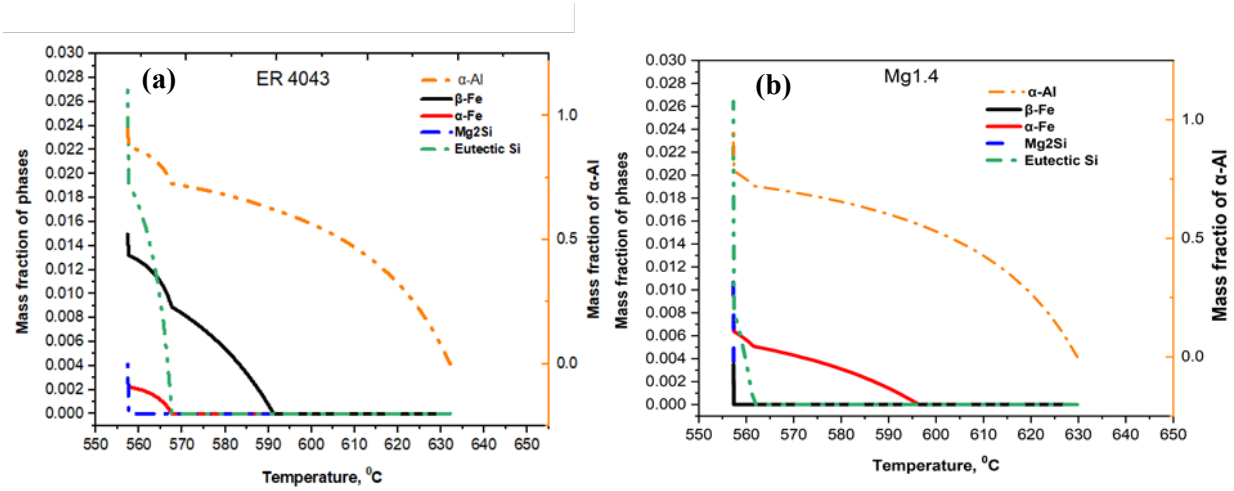

Figure 6: Predicted phase amounts of (a) ER4043 and (b) Mg1.4 joints under non-equilibrium Scheil condition.

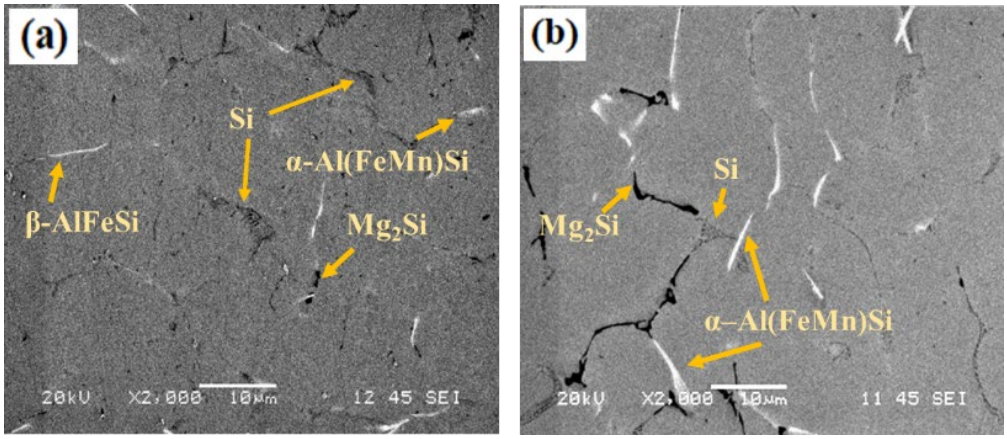

Figure 7: SEM images of the FZ of the (a) ER4043 and (b) Mg1.4 joints in the as-welded condition.

3.2.2 Mg distribution and the weld soundness

The variation in Mg concentration from the weld toe to the weld surface has been previously reported (Ref 13,14). Therefore, the Mg distribution in the FZs was investigated using SEM-EDS, and the results are presented in Fig. 8. The Mg concentrations at all the weld surfaces were lower, ranging between 0.2 to 0.29%. The Mg concentration at the weld toe of ER4043 was still relatively low (0.23%). However, at the weld toe of the joints of the new fillers, the Mg concentrations were remarkably higher, and reaching values of 0.72, 0.81, and 0.88% in the Mg0.6, Mg1, and Mg1.4 joints, respectively (Fig. 8(a)).

Furthermore, the Mg distributions from the weld cap to the weld root were analyzed, and the corresponding results are presented in Fig. 8(b). The Mg concentration at the weld roots was significantly higher than that at the weld caps. Overall, the Mg concentration in the FZ of the new fillers was much higher than those of ER4043, where the higher the Mg content of the fillers, the higher the Mg concentration in the FZ. Similar observations on the distribution of Mg in weld beads have been previously reported (Ref 15,16). The loss and nonuniform distribution of Mg in the FZs can be attributed to the evaporation and burning of Mg (Ref 13,14). Mg can readily evaporate from the weld pool surface due to its low boiling point (1090 °C). In addition, owing to the buoyancy force and lower density of Mg relative to Al, Mg can float to the top surface of the weld pool. Hence, Mg can be vaporized in the hot region of the weld pool surface, underneath the welding arc, and subsequently condense at the weld toes/sides. In the macroscopic view of the weld beads illustrated in Figs. 8(c)–(e), dark zones (i.e., black smut) were observed in the periphery of the weld beads. The darkness and area of the black smut correlated with the Mg content of the filler; the higher the Mg concentration of the fillers, the larger and darker were the black smuts. As previously reported, the black layer can be attributed to the oxidation of Mg (Ref 14,17).

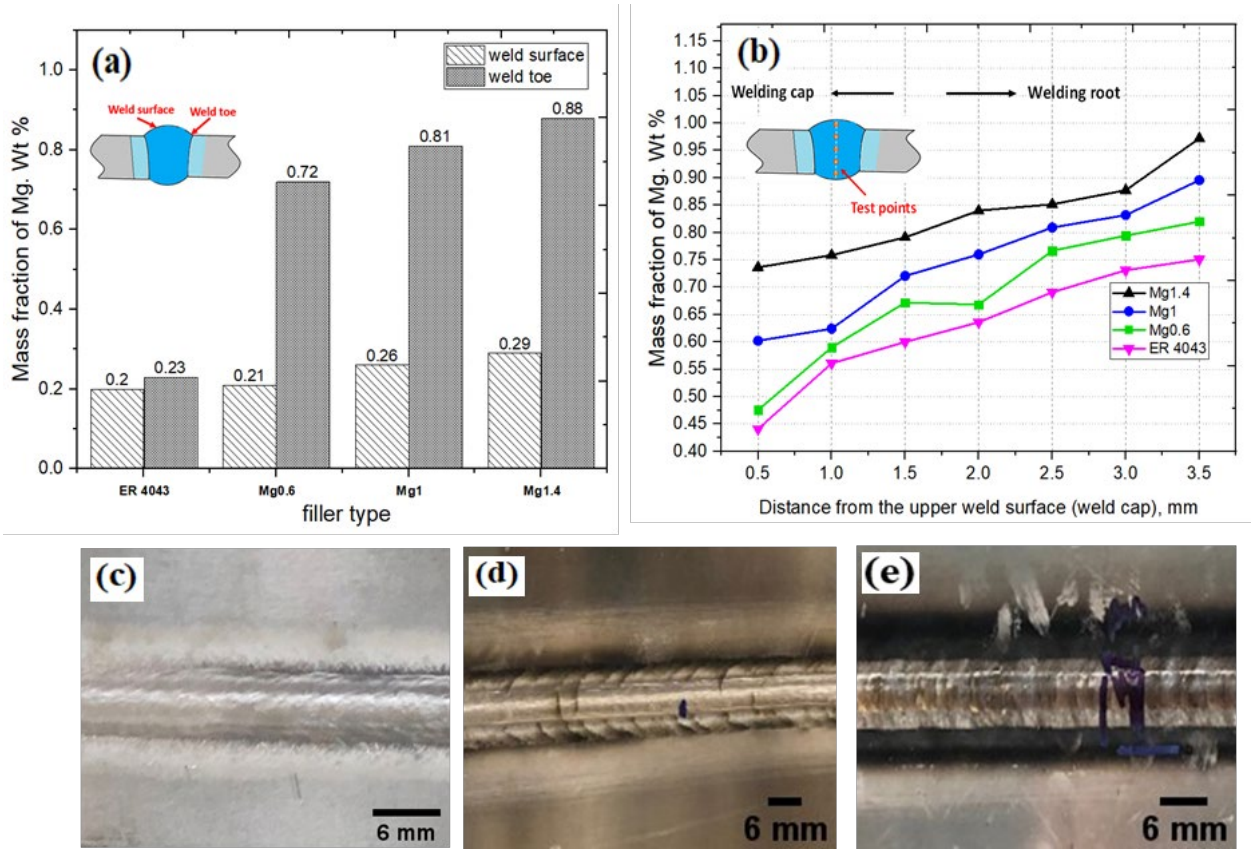

Figure 8: (a) Mg concentration at the weld surface and weld toe, (b) Mg distribution along the weld centerline and macro images of the black smut (Mg and Al oxides) around the weld bead in (c) ER4043, (d) Mg0.6, and (e) Mg1.4 joints.

3.2.3 PWHT microstructure

The microstructure of the FZ after PWHT is shown in Fig. 9. With the applied heat treatment, the Mg_2Si and eutectic Si particles were partially dissolved. The remaining Mg_2Si and Si particles, with plate-like morphology, were modified to a fibrous round structure. The dissolved particles can contribute to strengthening the FZ via solid solution and precipitation hardening (Ref 18). Furthermore, a slight fragmentation of the Fe-bearing intermetallics, marked with dotted circles in Fig. 9, was observed in the microstructure after the heat treatment.

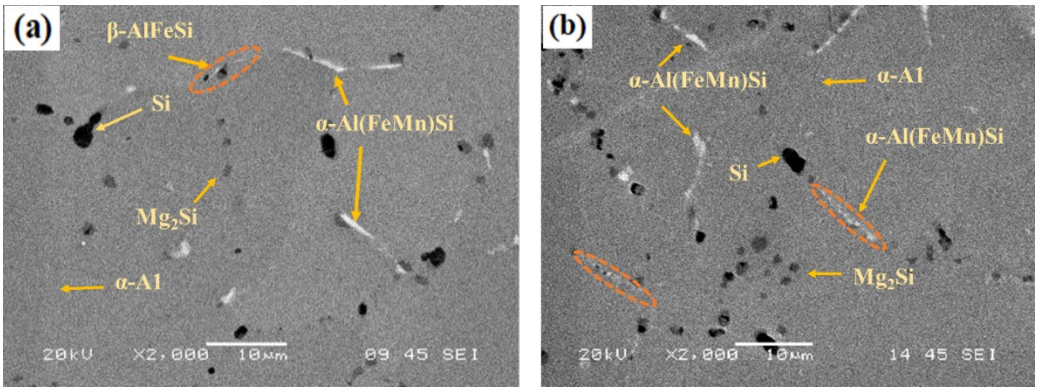

Figure 9: SEM images of the FZ in (a) ER4043 and (b) Mg1.4 joints after PWHT.

3.3 Mechanical properties

3.3.1 Microhardness measurement

The microhardness results of the as-welded joints along the central line across the FZ are shown in Fig. 10(a). The welded samples were divided into three distinct zones based on the HV results. The BM exhibited the highest hardness, with a constant profile (~120 HV), among all the welded samples. The HAZ appeared when the BM moved towards the FZ. Here, a remarkable reduction in HV was observed until reaching the minimum HV, and then the HV value increased again. In the HAZ, the HV values were similar for all welded samples. The large HV reduction in the HAZ can be attributed to recrystallization (Fig. 5(b)) and the dissolution/coarsening of strengthening precipitates (e.g., β"-Mg_2Si) in the BM owing to the arc heat input (Ref 11). With further movement from the HAZ (the softest zone) to the FZ, the HV sharply increased and reached a narrow plateau. The highest HV of the FZ was 115–120 HV for the Mg1.4 sample, similar to the HV of the BM. The HV values of the FZ were reduced to 107 and 104 for the Mg1 and Mg0.6 samples, respectively. The lowest HV of the FZ was 96 HV for the ER4043 sample, approximately 20% lower compared to that of the Mg1.4 sample. In the as-welded state, with increasing Mg content from 0.6% Mg (Mg0.6 filler) to 1.4% Mg (Mg1.4 filler), the Mg content in the FZ increased and hence high solid solution strengthening was obtained (Fig. 10(a)). Therefore, the HV improvement in the FZ by Mg addition is attributed to Mg solid solution hardening and possible natural aging prior to HV testing.

After the PWHT, the microhardness of the welded samples was again measured along the centerline of the FZ; the corresponding results are shown in Fig. 10(b). The microhardness of the BM was ~130 HV, slightly higher than the initial HV of the BM in the as-welded condition (~120 HV). This could be associated with the optimized heat treatment to reach the peak aging in this study. The lost HV of the HAZ was entirely recovered after the PWHT, ensuring that the BM and HAZ exhibited similar HV values. The HV profiles across the FZs were also significantly enhanced compared to those of the as-welded condition. For instance, the HV of the FZ in the ER4043 joint exhibited a 40% improvement (96 *vs*. 137 HV). In addition, the HV value of the ER4043 joint was slightly higher than that of the BM (137 *vs*. 130 HV), even though the Mg content in the BM was higher than that in the ER4043 joint. This result can be associated with the excess Si content in the FZ of ER4043 filler, through which a greater volume fraction of β"-Mg_2Si precipitates were formed (Ref 19,20), confirmed in Section 3.5. Furthermore, the HV values of the FZ welds with the three new fillers were remarkably higher than those of the BM and FZ welds of the ER4043 reference filler. The HV values of the FZs increased from 137 HV for the ER4043 joint to 143, 146, and 148 HV for the Mg0.6, Mg1, and Mg1.4 joints, respectively (Fig. 10(b)). In the PWHT condition, the primary Mg_2Si particles in the FZ were first dissolved, and then nanoscale β"-Mg_2Si precipitates were formed during aging, contributing HV enhancement with increasing Mg content in the filler metals via precipitation hardening.

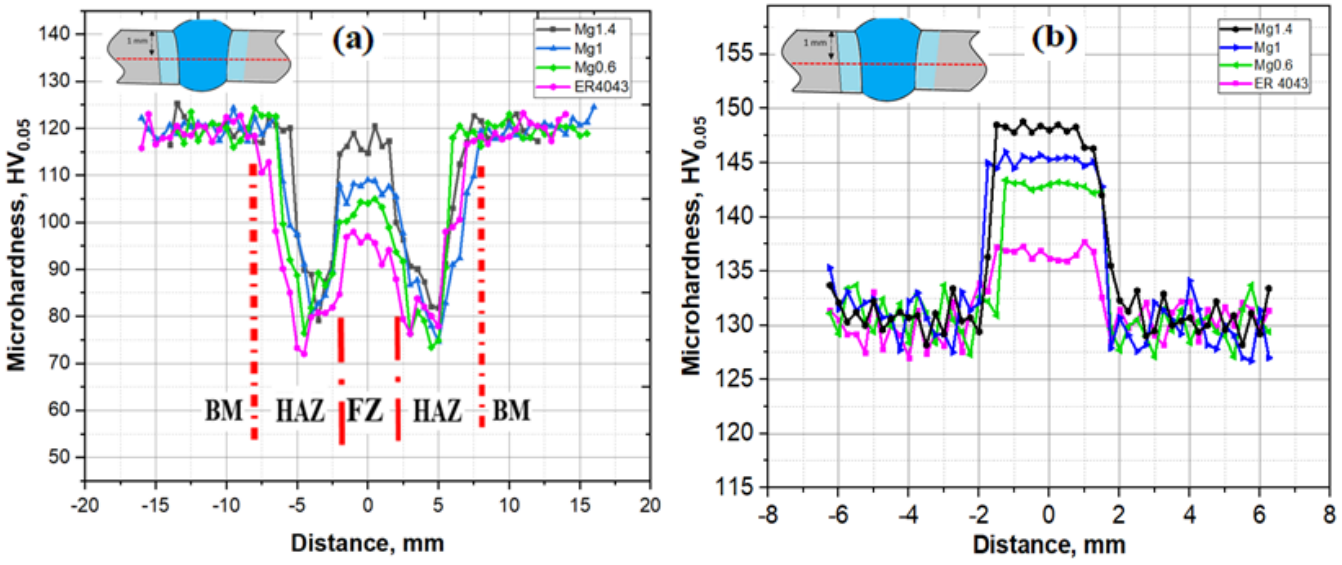

Figure 10: Microhardness profiles of the welded joints in (a) as-welded condition and (b) after PWHT.

3.4 Tensile properties

3.4.1 Tensile strengths of standard samples

The tensile strengths of all the welded samples are presented in Fig. 11. The yield strength (YS) and ultimate tensile strength (UTS) of the BM were 265 and 318 MPa, respectively. In the as-welded condition, all the welded samples with the four filler metals exhibited almost the same YS (~125 MPa) and UTS (~200 MPa), remarkably lower than those of the BM. A close look at the welded samples after tensile testing indicated that all the welded samples made with the four fillers were fractured in the HAZ (Fig. 11(b)), which was the softest zone according to the HV results (Fig. 10(a)), thus explaining the similar tensile strengths exhibited by all the welded samples. It is event that the as-welded tensile properties of all joints reflected only the minimum mechanical strength in the HAZ.

As shown in Fig. 11(a), the tensile strengths of weld samples with the four fillers were significantly enhanced after the PWHT and reached the same level of tensile strength of the BM (i.e., YS and UTS of ~275 and ~325 MPa, respectively). The fractures of all the weld samples were again outside the FZ but in the BM (Fig. 11(b)). The HV profiles along the welding samples (Fig. 10(b)) indicate that the strength of the HAZ was entirely recovered after PWHT, and the strength of the FZs made with the four fillers was remarkably higher than that of the BM. The fracture of welded samples occurs in the BM, thus explaining why all the welded samples, regardless of their Mg content, exhibited similar tensile properties as the BM and achieved 100% welding efficiency (UTS_{joint} / UTS_{BM} x 100).

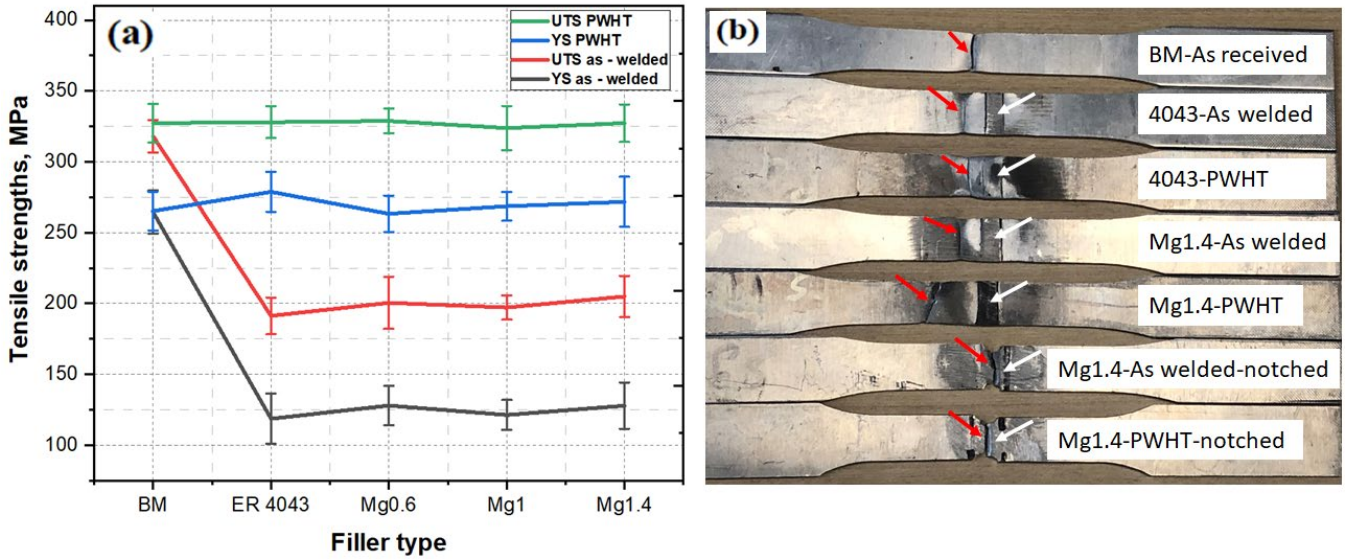

Figure 11: (a) Tensile strengths of the standard samples and (b) macro-images of fractured tensile samples under different conditions. The white and red arrows indicate the FZs and the fractures, respectively.

3.4.2 Tensile strengths of notched samples

As mentioned previously, the standard tensile samples fractured either in the HAZ in the as-welded condition or in the BM in the PWHT condition. Tensile tests in the FZ were conducted with double-edge notched samples to better understand the impact of the elemental contributions (i.e., the Mg content) on the weld bead strength (Fig. 2(b)). A correction factor (Ref 21,22) was applied to correlate the tensile properties of the notched samples to those of the standard tensile samples to obtain the tensile strengths of the FZ. The tensile strengths of the FZs in as-welded condition are shown in Fig. 12(a). Due to the reduced area of the FZs in the notched tensile samples, all the fractures were located in the FZ (Fig. 11(b)). The YS and UTS values of the FZ welded with the reference filler reached 148 and 238 MPa, respectively, already higher than that of the HAZ (black and red dashed lines in Fig. 12(a)). With increasing Mg content, the YS of the FZ made with the new fillers increased up to 179 MPa for the Mg1.4 filler, 20% higher than that of the FZ welded by the reference filler. Similar, the UTS of the FZ welded by the new fillers

was also improved with increasing the Mg content. For instance, the UTS of the FZ made with Mg1.4 filler reached 260 MPa, 10% higher than that of the FZ made with the reference filler. These improvements in tensile strength, consistent with the microhardness results (Fig. 10(a)), are mainly attributed to the increased solid solution strengthening of the FZ induced by the higher Mg content in the new fillers (Ref 23).

Subsequently, the mechanical strength was evaluated after PWHT, and the results for the notched samples are shown in Fig. 12(b). The YS and UTS of the FZ made with the reference filler was 288 MPa and 340 MPa, respectively, exceeding the YS and UTS of the BM (275 MPa and 325 MPa, respectively, as marked by the blue and green dashed lines in Fig. 12(b)). Among the four filler metals, the reference filler exhibited the lowest tensile strength. The tensile strengths of the PWHT joints welded with the new fillers were remarkably higher than those of the joints made with the reference filler. For instance, the joint made with the Mg1.4 filler exhibited a YS of 336 MPa and UTS of 392 MPa. The higher the Mg content in the filler metals, the higher the tensile strengths of the joints, consistent with the HV results presented in Fig. 10(b).

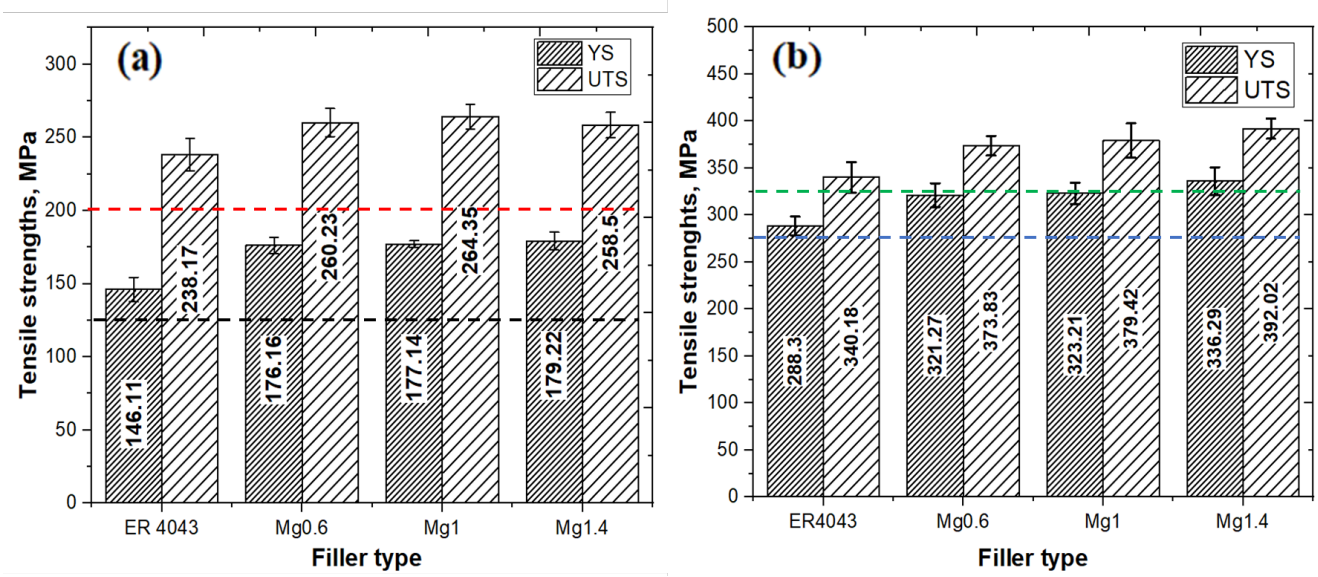

Figure 12: Tensile strengths of the notched samples in (a) as-welded and (b) PWHT conditions. The black and red dash lines in (a) represent the YS and UTS of the standard samples in the as-welded condition, while the blue and green dash lines in (b) show the YS and UTS of the standard samples in the PWHT condition.

3.5 TEM analysis

The HV and tensile results (Fig. 10(a) and 10(a)) indicated that the HAZ was the softest zone in all the as-welded samples. Therefore, TEM analysis was conducted to characterize the precipitate microstructure in the HAZ and the BM. The bright-field TEM image in Fig. 13(a) reveals the precipitate microstructure of the BM. It can be seen that very fine and needle-shaped β"-Mg_2Si precipitates were uniformly distributed in the α-Al matrix of the BM, which are the main strengthening phase in AA6061-T6 aluminum plates. Fig. 13(b), taken at ~2 mm from the fusion line of the Mg1.4 joint, the approximate softest point in the HAZ (Fig. 10(a)), indicated that most of the fine and coherent β"-Mg_2Si was transformed to equilibrium and large β-Mg_2Si particles in the matrix as a result of exposure to high temperature (Ref 24,25). Therefore, the strengthening effect on the aluminum matrix was almost completely lost. With increasing distance from the FZ, the effect of the arc heat input during welding was reduced. Fig. 13(c), taken at ~7 mm from the fusion line of the Mg1.4 joint, showed that the fine and coherent β"-Mg_2Si were transformed into coarse and semi-coherent β'-Mg_2Si precipitates, resulting in a partial loss of the strengthening effect. In addition, the grains in the HAZ were mostly recrystallized due to the effect of the arc heat input (Fig. 5(b)). The microstructure evolution in the HAZ, related to the heat flux during welding, accounts for the softening of the HAZ, resulting in the weakest zone in all the as-welded samples.

The precipitate microstructure in the FZ of the PWHT samples was investigated using TEM. Typical results for the FZ made with the ER4043, Mg0.6, and Mg1.4 fillers are presented in Fig. 14(a) to (c). The quantitative

results of the number densities and volume fractions of the β"-Mg_2Si precipitates in the BM and all the welded samples are shown in Fig. 14(d). The microstructures of the FZs in all the welded samples were dominated by nanosized and coherent β"-Mg_2Si precipitates (Fig. 14(a)). The FZ of the reference filler had a slightly higher number density and volume fraction of precipitates than the BM (Fig. 13(a)), although the BM had a higher Mg content, attributed to the higher excess Si content in the ER4043 joint, promoting the formation of β"-Mg_2Si precipitates (Ref 19). With increasing Mg content in the new fillers, the β"-Mg_2Si precipitates became finer (Fig. 14(b) and (c)), and the number density and volume fraction of precipitates increased (Fig. 14(d)). Therefore, compared to the BM and the reference filler joint, the higher HV (Fig. 10(b)) and greater tensile strength (Fig. 12(b)) of the FZs of the new fillers were directly related to the finer and denser β"-Mg_2Si precipitates. After the PWHT, the HAZ of the welded samples recovered to the original strength of the BM. However, the FZs welded by the new fillers became much stronger; hence, the weld beads are no longer the limiting factor for the overall strength of the welded components, thus indicating the significant potential for the welding of high-strength aluminum structures.

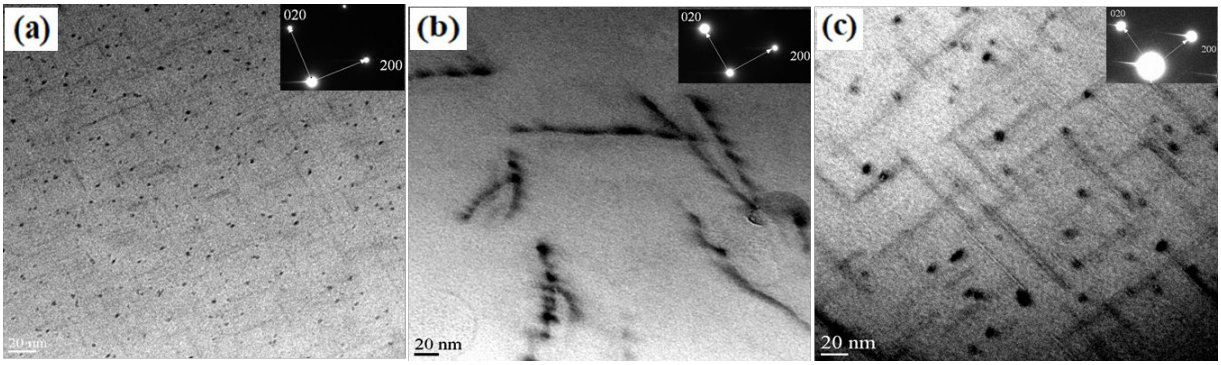

Figure 13: Bright-field TEM images of (a) β" precipitates in BM, (b) β precipitates at 2 mm from the fusion line, and (c) β' precipitates at 7 mm from the fusion line in the Mg1.4 joint.

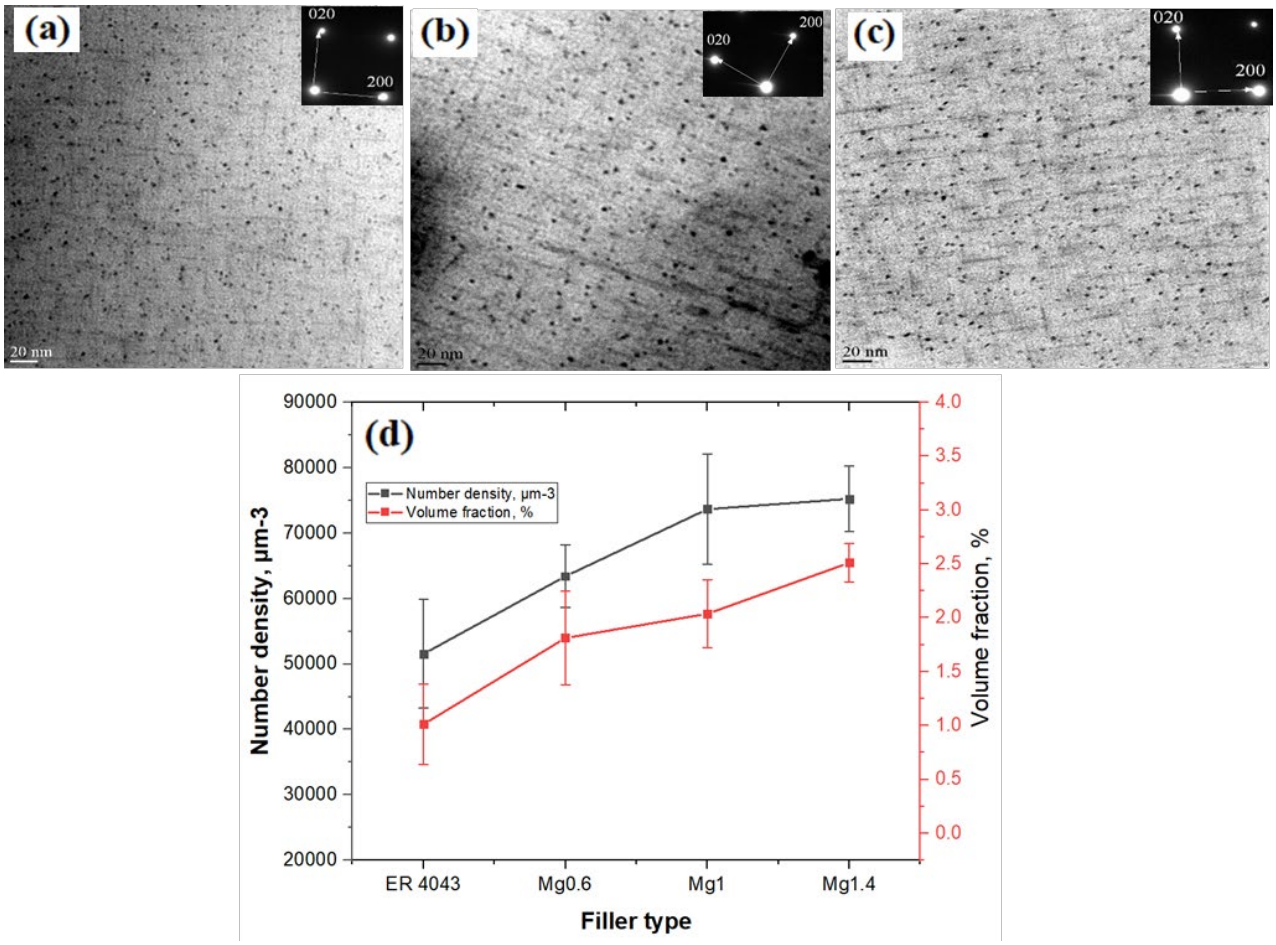

Figure 14: Bright-field TEM images of β" precipitates in the FZs of (a) ER4043, (b) Mg0.6, (c) Mg1.4 joints. (d) Quantitative results of the β" precipitates.

4. Conclusions

1) The new Al-Si-Mg 4xxx filler metals exhibited weldability similar to that of the ER4043 commercial filler. No slag inclusions, oxides, cracks, lack of fusion, or incomplete penetration were observed for any of the welded plates.
2) In the joints of all the filler metals, the Mg concentration varied significantly from the weld surface to the weld toe and from the weld root to the weld cap. The average Mg concentration in the FZ of the new fillers was much higher than that of the reference filler, increasing with increasing Mg content in the new fillers.
3) In the as-welded condition, all the welded samples exhibited similar mechanical strength, but much lower than the BM. The strength of the FZ was greater than the minimum strength of the HAZ for any given filler. Therefore, all the welded samples were fractured at the HAZ, the weakest zone in the joints owing to recrystallization and the dissolution/coarsening of the strengthening precipitates.
4) After applying the PWHT, the mechanical strength of all joints, regardless of the Mg content, reached the same level as the BM, achieving 100% welding efficiency.
5) The results of the microhardness and notched tensile samples indicated that although the HAZ of the welded samples was recovered during PWHT, the FZs welded by new fillers became much stronger than the BM and the joint made by the reference filler, thus indicating the significant potential for the welding of high-strength aluminum structures. The improved strength of the FZs was attributed mostly to the finer and denser β"-Mg_2Si owing to the higher Mg content in the FZs made by new fillers compared to that made by the reference filler.

Acknowledgments

The authors would like to acknowledge the financial support from the Natural Sciences and Engineering Research Council of Canada (NSERC) and Rio Tinto Aluminum under the Grant No. CRDPJ 514651-17 through the Research Chair in Metallurgy of Aluminum Transformation at the University of Quebec at Chicoutimi.

References

1. W. Miller, L. Zhuang, J. Bottema, A.J. Wittebrood, P. De Smet, A. Haszler, and A. Vieregge, Recent Development in Aluminium Alloys for the Automotive Industry, *Mater. Sci. Eng., A,* 2000, **280**(1), p 37-49
2. J.S. Pérez, R.R. Ambriz, F.F.C. López, and D.J. Vigueras, Recovery of Mechanical Properties of a 6061-T6 Aluminum Weld by Heat Treatment after Welding, *Metall. Mater. Trans. A,* 2016, **47**(7), p 3412-3422
3. A. Lakshminarayanan, V. Balasubramanian, and K. Elangovan, Effect of Welding Processes on Tensile Properties of Aa6061 Aluminium Alloy Joints, *Int. J. Adv. Manuf. Technol.,* 2009, **40**(3), p 286-296
4. A.W. AlShaer, L. Li, and A. Mistry, Effect of Filler Wire Properties on Porosity Formation in Laser Welding of Ac-170px Aluminium Alloy for Lightweight Automotive Component Manufacture, *Proc Inst Mech Eng B J Eng Manuf,* 2017, **231**(6), p 994-1006
5. I. Guzmán, E. Granda, J. Acevedo, A. Martínez, Y. Dávila, and R. Velázquez, Comparative in Mechanical Behavior of 6061 Aluminum Alloy Welded by Pulsed Gmaw with Different Filler Metals and Heat Treatments, *Materials,* 2019, **12**(24), 4157
6. B. Anderson, T. Anderson, G. White, and P. Berube, A New Development in Aluminum Welding Wire: Alloy 4943, *Weld. J.,* 2013, **92**(7), p 32-37
7. Anderson, Stephen L, Anderson, Bruce E, Aluminum Welding Filler Metal, Casting and Wrought Metal Alloy (U.S. Patent No. 2015/0132181 A1) , 2015.
8. N.K. Babu, M.K. Talari, D. Pan, Z. Sun, J. Wei, K.J.M.C. Sivaprasad, and Physics, Microstructural Characterization and Grain Refinement of AA6082 Gas Tungsten Arc Welds by Scandium Modified Fillers, 2012, **137**(2), p 543-551
9. N.K. Babu, M.K. Talari, P. Dayou, S. Zheng, W. Jun, and K. SivaPrasad, Influence of Titanium–Boron Additions on Grain Refinement of AA6082 Gas Tungsten Arc Welds, *Mater. Des.,* 2012, **40**, p 467-475
10. Aluminum Filler Alloy Selection Chart, (AlcoTec Wire Corporation) http://alcotec.com/us/en/support/upload/Aluminum_Filler_Alloy_Selection_Chart.pdf, 2015.
11. Y. Liang, J. Shen, S. Hu, H. Wang, and J. Pang, Effect of Tig Current on Microstructural and Mechanical Properties of 6061-T6 Aluminium Alloy Joints by Tig–CMT Hybrid Welding, *J. Mater. Process. Technol.,* 2018, **255**, p 161-174
12. Technical committee ISO/TC 44, Welding - Arc-Welded Joints in Aluminium and Its Alloys - Quality Levels for Imperfections, ISO 10042:2005(E), ISO, 2005, p 1-27
13. T.E. Borchers, D.P. McAllister, and B. Zhang, Macroscopic Segregation and Stress Corrosion Cracking in 7xxx Series Aluminum Alloy Arc Welds, *Metall. Mater. Trans. A,* 2015, **46**(5), p 1827-1833
14. H.-k. Lee, T.-j. Yoon, and C.-y. Kang, Analysis of Smut Formation Phenomena on Mig and Plasma-Mig Hybrid Weld of Cryogenic Al-Mg Alloy, *J. Korean Inst. Met. Mater,* 2016, **54**(2), p 79-88
15. X. Zhan, J. Chen, J. Liu, Y. Wei, and J.M. Zhou, Microstructure and Magnesium Burning Loss Behavior of Aa6061 Electron Beam Welding Joints, *Mater. Des.,* 2016, **99**, p 449-458
16. L. Zhou, M. Zhang, X. Jin, H. Zhang, and Mao, Study on the Burning Loss of Magnesium in Fiber Laser Welding of an Al-Mg Alloy by Optical Emission Spectroscopy, *Int. J. Adv. Manuf. Technol.,* 2017, **88**(5-8), p 1373-1381

17. H.-K. Lee, K.-S. Chun, S.-H. Park, and C.-Y. Kang, Control of Surface Defects on Plasma-Mig Hybrid Welds in Cryogenic Aluminum Alloys, *Int. J. Nav. Archit. Ocean Eng,* 2015, **7**(4), p 770-783

18. J.-h. Peng, X.-l. Tang, J.-t. He, and D.-Y. Xu, Effect of Heat Treatment on Microstructure and Tensile Properties of A356 Alloys, *Trans. Nonferrous Met. Soc. China,* 2011, **21**(9), p 1950-1956

19. A. Gupta, D. Lloyd, and S.J.M.S. Court, Precipitation Hardening in Al–Mg–Si Alloys with and without Excess Si, *Mater. Sci. Eng., A,* 2001, **316**(1-2), p 11-17

20. J. Rakhmonov, K. Liu, P. Rometsch, N. Parson, and X. Chen, Improving the Mechanical Response of Al–Mg–Si 6082 Structural Alloys During High-Temperature Exposure through Dispersoid Strengthening, *Materials,* 2020, **13**(22), p 5295

21. J. Choung, and S. Cho, Study on True Stress Correction from Tensile Tests, *J. Mech. Sci. Technol,* 2008, **22**(6), p 1039-1051

22. V. Olden, Z. Zhang, E. Østby, B. Nyhus, and C. Thaulow, Notch Tensile Testing of High Strength Steel Weldments, 2nd international symposium on high strength steel, 2002

23. O. Myhr, Ø. Grong, H. Fjær, and C. Marioara, Modelling of the Microstructure and Strength Evolution in Al–Mg–Si Alloys During Multistage Thermal Processing, *Acta Mater.,* 2004, **52**(17), p 4997-5008

24. L. Zhang, X. Li, Z. Nie, H. Huang, and J. Sun, Softening Behavior of a New Al-Zn-Mg-Cu Alloy Due to Tig Welding, *J. Mater. Eng. Perform.,* 2016, **25**(5), p 1870-1879

25. M. Peel, A. Steuwer, and P. Withers, Dissimilar Friction Stir Welds in AA5083-AA6082. Part II: Process Parameter Effects on Microstructure, *Metall. Mater. Trans. A,* 2006, **37**(7), p 2195-2206